Food & Function

ROYAL SOCIETY OF CHEMISTRY

PAPER

View Article Online
View Journal

Cite this: DOI: 10.1039/d6fo00323k

Crossing and metabolism of tyrosol and hydroxytyrosol by implementing an *in vitro* blood–brain barrier model of human primary cells

Sonia Gulabrai-Díaz, [a] Blanca Escudero-López,[b] Carmen del Río, [c,d] Joan Montaner,[c,e] Marta Berzaghi,[f] Pedro Mena, [f] Ana M Troncoso [a] and Ruth Hornedo-Ortega *[a]

There is mounting evidence that the neuroprotective benefits associated with olive oil consumption are related to the presence of the phenolic alcohols tyrosol (Tyr) and hydroxytyrosol (HT). *In vitro* blood–brain barrier (BBB) models are considered indispensable platforms for the mechanistic assessment of compound permeability. However, it is important to note that most of these models offer only a limited representation of BBB physiology. The aim of the present study was to develop a human triculture (human brain microvascular endothelial cells (HBMECs), astrocytes and pericytes) BBB model to evaluate the permeability of dietary bioactives. In particular, the crossing of Tyr and HT through the BBB and the BBB's potential to further metabolize these bioactives were evaluated. Different seeding densities of HBMECs and the presence/absence of fibronectin as extracellular matrix were considered. 1×10^5 cells and fibronectin coating of the apical transwell surface yielded higher TEER values and improved barrier integrity. Immunocytochemical analysis further confirmed the well-defined ZO-1 localisation at the cell–cell junctions. After 96 h of the establishment of the triculture, the human-origin BBB (ho-BBB) model presented the optimal barrier conditions for the execution of permeability studies. The transport of Tyr and HT (at two different concentrations, 1 and 10 μM) across the ho-BBB was evaluated by UPLC-MS/MS. Our results proved that the ho-BBB was more permeable to HT (high permeability) than Tyr (medium permeability), as determined by calculating transport percentages and apparent permeability coefficients (P_{app}). This study provides the first evidence that HBMECs can metabolize HT, transforming it into HT-3′-sulfate and HT-4′-sulfate.

Received 21st January 2026,
Accepted 18th March 2026

DOI: 10.1039/d6fo00323k

rsc.li/food-function

Introduction

The Mediterranean diet has been strongly associated with the prevention of numerous non-communicable diseases including neurodegenerative disorders.[1,2] Such an interplay between nutrition and health has attracted attention towards food bioactives. In particular, the main dietary source of lipids in the Mediterranean diet, olive oil, has drawn special interest, not only for its high proportion of oleic acid but also for the content of (poly)phenols in its unsaponifiable fraction. These compounds stand out as major contributors to the health-promoting properties of this product,[3,4] and they can largely vary from 0.02 to 600 mg kg^{-1} oil, depending on the olive cultivar, growing conditions, and oil extraction processes and techniques.[5–8] Thus, extra virgin olive oil (EVOO), produced exclusively through mechanical processes, possesses the highest content of (poly)phenols.[9,10]

Quantitatively, the most abundant phenolics in EVOO are the phenyl alcohols hydroxytyrosol (HT, 2-(3′-4′-dihydroxyphenyl)ethanol, from 0.6 to 200 mg kg^{-1}) and tyrosol (Tyr, 2-(4′-hydroxyphenyl)ethanol, from 1.1 to 180 mg kg^{-1}),[11,12] together with various secoiridoid derivatives such as oleuropein, oleacein, oleocanthal, and ligstroside.[13] Oleuropein, the predominant glycoside in the olive fruit, undergoes hydrolytic degradation to yield HT and elenolic acid, making HT the principal degradation product of oleuropein in EVOO. Similarly, Tyr is

[a]*Departamento de Nutrición y Bromatología, Toxicología y Medicina Legal. Facultad de Farmacia, Universidad de Sevilla, c/P García González, no 2, 41012 Sevilla, Spain. E-mail: rhornedo@us.es*
[b]*Área de Nutrición y Bromatología, Departamento de Biología Molecular e Ingeniería Bioquímica, Universidad Pablo de Olavide, Carretera de Utrera Km 1, 41013 Sevilla, Spain*
[c]*Instituto de Biomedicina de Sevilla, IBiS, Hospital Universitario Virgen del Rocío, CSIC, Universidad de Sevilla, 41013 Sevilla, Spain*
[d]*Departamento de Biología Celular, Facultad de Biología, Universidad de Sevilla, 41013 Sevilla, Spain*
[e]*Department of Neurology, Hospital Universitario Virgen Macarena, 41004 Sevilla, Spain*
[f]*LS9 Bioactives and Health Interlab Group and Human Nutrition Unit, Department of Food Science, University of Parma, Via Volturno 39, 43125 Parma, Italy*

mainly derived from the breakdown of ligstroside, further highlighting the close metabolic relationship among these key phenolic constituents.[8,14,15]

In recognition of their biological relevance, the European Food Safety Authority (EFSA) approved the health claim that olive oil (poly)phenols, particularly HT and its derivatives, contribute to the protection of blood lipids from oxidative stress, when consumed at a minimum daily intake of 5 mg of HT per 20 g of olive oil.[16] Pastor *et al.* (2016)[17] found that free HT was undetectable in plasma after the ingestion of 25 mL of regular olive oil and reached a maximum of 4.4 ng mL^{-1} following the consumption of 25 mL of EVOO, thus reflecting low HT concentrations in plasma. The total amount of HT entering systemic circulation was estimated to be 3.98 μg, representing 0.3% of the administered dose. This is largely due to an extensive phase II metabolism, with free HT accounting for only 0.1–1% of the total HT metabolites in plasma.[17]

A growing body of evidence from observational studies suggests that the neuroprotective effects associated with the Mediterranean diet are largely attributable to olive oil (poly) phenols, particularly HT and its derivatives.[18–20] These compounds have been linked to a reduced risk of cognitive decline and neurodegenerative diseases, such as Alzheimer's and Parkinson's disease, as well as to improvements in cognitive performance.[21,22] The blood–brain barrier (BBB) is a highly selective permeable barrier that separates circulating blood from brain extracellular fluid in the central nervous system, which is primarily composed of microvascular endothelial cells, astrocytes, pericytes, and neurons.[23,24]

Interestingly, a recent work has demonstrated the presence of tyrosols in human cerebrospinal fluid, pointing out the possibility for these bioactives to reach the BBB.[25]

Evidence indicates that HT is present in the brain (and other organs and tissues) in a dose-dependent manner following its oral administration in rats.[26–28] In addition, certain metabolites of HT and Tyr have been shown to cross the BBB in rats, namely, HT-sulfate, HT-acetate-sulfate, and Tyr-sulfate.[29] The ability of HT and Tyr to cross the BBB has also been demonstrated using *in vitro* methods, specifically, using HBMECs in monoculture and, very recently, using a BBB hypoxia model in triculture.[30,31] The low molecular weight of these compounds (less than 500 Da) and their low hydrogen bond formation potential could provide an explanation for the greater ability of these metabolites to cross the BBB.[32]

To investigate the potential transport of (poly)phenols across the BBB, a great variety of experimental and computational approaches have been used. *In silico* models, including numerical and computational simulations and machine learning algorithms, allow prediction of BBB penetration based on molecular properties and large datasets, providing a fast and cost-effective complement to experimental studies.[33] *In vitro* models offer controlled experimental systems that range from simple static cultures, including monocultures and co-cultures in transwell systems,[30,33] to more complex three-dimensional approaches such as spheroids and organoids.[34,35] Moreover, parallel artificial membrane permeability assay (PAMPA) provide a rapid, high-throughput, and cell-free method to estimate passive permeability through a lipid-infused artificial membrane.[36] *In vivo* models, typically involving rodents or other animals, allow assessment of BBB permeability within the context of a living organism, capturing systemic metabolism, transport mechanisms, and tissue interactions. However, substantial interspecies variability limits the direct extrapolation of these results to clinical outcomes.[37–39] Together, these approaches offer a comprehensive toolkit for studying the transport of food bioactives across the BBB, each with distinct advantages and limitations, and inform the selection of the most suitable model for mechanistic or screening studies.

The utilisation of *in vitro* models is gaining popularity due to their capacity to rapidly evaluate the potential effects of bioactive substances and to assess the efficacy of varying concentrations.[40] *In vitro* models that can accurately mimic the BBB in culture are critical tools for studying drug/compound permeability. Among all of them, monocultures of brain microvascular endothelial cells (BMECs) on transwell systems have been widely utilised for assessing phenolic compounds due to their simplicity, reproducibility, and ease of handling.[30,33,41,42] However, these simplified systems are not capable of accurately reproducing the structural and functional complexity of the BBB, particularly its tight junction integrity and dynamic interactions with the surrounding neural environment. It is for this reason that co-culture models incorporating astrocytes and/or pericytes have gained prominence, as these cell types play essential roles in the induction and maintenance of BBB integrity, the regulation of endothelial permeability, and the development of functional tight junctions.[43–45] Consequently, the objective of this study was to evaluate the permeability of dietary bioactive compounds by implementing a human-origin triple co-culture BBB model (ho-BBB) as a more realistic *in vitro* system. The study also sought to determine the potential metabolic activity of the BBB to form new brain metabolites.

Experimental

Chemicals and reagents

Hydroxytyrosol (HT) (purity ≥ 90%, CAS number: 10597-60-1), tyrosol (Tyr) (purity ≥ 98%, CAS number: 501-94-0) and dimethyl sulfoxide (DMSO) were acquired from Sigma Aldrich (St Louis, MO, USA). Hydroxytyrosol-3′-sulfate sodium salt (purity ≥ 95%, CAS number: 1391053-88-5) and hydroxytyrosol-4′-sulfate sodium salt (purity ≥ 95%, CAS number: 1817821-22-9) were provided by LGC Standards (Teddington, Middlesex, UK). Hydroxytyrosol-3′-glucuronide (purity ≥ 98%, CAS number: 425408-50-0), hydroxytyrosol-4′-glucuronide sodium salt (purity ≥ 95%) and tyrosol-sulfate sodium salt (purity ≥ 95%, CAS number: 28116-27-0) were purchased from Santa Cruz Biotechnology (Dallas, Texas, USA).

Cell culture conditions

Primary human astrocytes, brain vascular pericytes and their specific cell culture media were obtained from ScienCell (Carlsbad, USA). Primary human brain microvascular endothelial

cells (HBMECs), their cell culture medium and bovine fibronectin were acquired from InnoProt (Bizkaia, Spain). Transwell inserts 3.0 μm, 12 mm and T75 flasks were supplied by Corning (New York, NY, USA). Poly-L-lysine, phosphate-buffered saline solution (10×), trypsin, and fetal bovine serum were purchased from Thermo Fisher Scientific (Waltham, MA, USA).

All cells were cultured in 75 cm^2 culture flasks containing 10–12 mL of their respective cell culture media supplemented with 1% (v/v) specific growth factors, 1% (v/v) penicillin/streptomycin solution and 2% (v/v) foetal bovine serum, all provided with the cell culture media. Cells were maintained at 37 °C in a humid atmosphere enriched with 5% CO_2. When cells reached 90% confluence, they were subcultured using 0.05% (astrocytes and pericytes) or 0.25% (HBMECs) trypsin-EDTA.

Cell characterization

First, the characterization of cells was achieved by the immunostaining of the platelet endothelial cell adhesion molecule (CD-31/PECAM-1), glial fibrillary acidic protein (GFAP) and platelet-derived growth factor receptor beta (PDGFRβ) for HBMECs, astrocytes, and pericytes, respectively.

For this purpose, 5×10^4 cells were seeded on round coverslips with the same area as the insert membrane (1.12 cm^2). The medium was discarded, and cells were fixed with a 4% (w/v) paraformaldehyde solution (Merck Millipore, Darmstadt, Germany) for 15 min at 4 °C and then washed with a phosphate-buffered saline (PBS) solution (Thermo Fisher Scientific).[33] To start off the immunofluorescence protocol, cells were permeabilized with a 0.1% Triton X-100 (Sigma Aldrich) solution in PBS (PBST) for 30 min and blocked in 5% bovine serum albumin (BSA, Sigma Aldrich) in PBST for 1 h at room temperature. Afterwards, incubation with each primary antibody in 1% BSA in PBST was performed overnight at 4 °C (Table 1A). Cells were then washed and incubated with secondary Alexa FluorTM antibodies (Table 1B) in 1% BSA in PBST for 2 h at room temperature prior to the addition of a 4′,6-diamidino-2-phenylindole (DAPI) 1 : 1000 (Thermo Fisher Scientific) nuclei staining solution for 5 min. Cells were then washed with PBS and mounted onto slides with a 50% glycerol solution. Confocal fluorescence images were obtained using a Leica Stellaris 8 Falcon confocal microscope with a 40× air objective.[46]

Table 1 Antibodies for immunofluorescence

Antibody	Company	Concentration
A. Primary antibodies for cellular characterization		
Rabbit anti-CD-31	Abclonal (A0378)	1 : 250
Mouse anti-GFAP	Sigma-Aldrich (MAB360)	1 : 500
Rabbit anti-PDGFRβ	Sigma-Aldrich (051135)	1 : 500
B. Secondary antibodies for cellular characterization		
Ac Donkey anti-Rb IgG AlexaFluor 546	Thermo Fisher Scientific (A10040)	1 : 500
Ac Donkey anti-Ms IgG AlexaFluor 647	Thermo Fisher Scientific (A31571)	1 : 500
C Primary antibodies for model functionality		
Rabbit anti-CD-31	Abclonal (A0378)	1 : 250
Rabbit anti-ZO-1	Sigma-Aldrich (SAB5700692)	1 : 200

Setup protocol for a triculture BBB model based on human cells

The development of the BBB model in triculture was based on a previous study by Stone *et al.* (2019).[44] The configuration used consisted of a mixed contact coculture between astrocytes and pericytes on the basolateral side of the insert and HBMECs on the apical side, as this setup has already shown the highest TEER values and, therefore, barrier integrity. As a novelty, the effect of different densities of HBMECs (7.5×10^4, 1×10^5, and 1.5×10^5 cells) and the absence or presence of fibronectin as an extracellular matrix for culture on the inserts of the latter were studied.

Astrocyte seeding. On day 1, the basolateral side of the inserts were coated with a poly-L-lysine solution (2 μg mL^{-1}) for 1 h in the incubator. After this time, the inserts were washed with a sterile PBS solution and turned upside down. Then, 100 μL of an astrocyte suspension containing 3.13×10^5 astrocytes was pipetted onto the basolateral side of the insert. The plates containing the seeded inserts were returned to the incubator for at least 3 h, leading to cell adhesion. After this time, the plates were removed from the incubator and flipped back. Both compartments were filled with the astrocyte cell culture medium (0.8 mL and 1 mL in the apical and basolateral compartments, respectively), and the plates were returned to the incubator until the next day.

Pericyte seeding. On the following day, the plates containing the inserts were removed from the incubator, and the cell culture medium was aspirated. Again, the inserts were turned upside down, and 100 μL of the pericyte suspension containing 6.25×10^4 pericytes was pipetted onto the basolateral side of the insert. An approximate 5 : 1 ratio between astrocytes and pericytes was obtained, according to Stone *et al.*'s (2019)[44] experience. Then, the plates were introduced in the incubator for another 3 h to ensure cell adhesion. After this time, the plates were removed from the incubator, and the inserts were flipped back. Both compartments were filled with the same volume described before of a 1 : 1 solution containing both astrocyte and pericyte cell media (mixed cell culture medium). The plates were returned to the incubator until the following day.

Fibronectin coating. On day 3, no cells were seeded, so that astrocytes and pericytes could reach an approximately 90% confluency. Nevertheless, the plates were removed from the incubator, and the cell culture medium in the apical compartment was aspirated. This side of the inserts was coated with a bovine fibronectin solution (2 μg mL^{-1}) for 24 h.

HBMEC seeding. On the last day of the model setup, HBMECs were seeded on the apical side of the insert. The plates inside the incubator were taken out, and fibronectin was aspirated. A 100 μL suspension containing 7.5×10^4, 1×10^5, or 1.5×10^5 HBMECs was added to the apical side. Cells were incubated for 5 h before topping the upper compartment with the endothelial cell culture medium (0.8 mL) and renewing the mixed culture medium in the basolateral compartment.

This marks day 1 of the triculture model. Cell culture media in both the apical and basolateral compartments were renewed every day until day 4, on which day permeability assays were performed.

Model functionality tests

Transendothelial electrical resistance (TEER) measurements. TEER measurements were performed every day to assess the optimal day for further permeability assays. An EVOM2 meter connected to STX3 electrodes (World Precision Instruments, Sarasota, FL, USA) was used. To ensure consistency, TEER measurements should always be read at least 24 h after medium renewal, and electrodes should be sterilized in 70% ethanol, followed by immersion in the cell culture medium for up to 15 min.

The STX3 electrodes were introduced in the insert. The longer end of the electrode was placed inside the basolateral compartment and adjusted to slightly touch the bottom of the plate. The shorter end was placed inside the apical compartment, avoiding direct contact with the membrane. The system reversed polarity in order to prevent electrode polarization, ion accumulation and tissue damage. TEERs were measured when values were stable. It is important to note that the insert on its own has a TEER value, which we used as a blank measurement. TEER values were calculated as follows:

$$\mathrm{TEER_{value}} = \mathrm{TEER_{measured}} - \mathrm{TEER_{blank}}.$$

Finally, as TEER measurements were expressed in $\Omega\ \mathrm{cm}^{-2}$, a correction regarding the area of the membrane was performed, being 1.12 cm^2 the total area of the membrane:

$$\mathrm{TEER_{reported}} = \mathrm{TEER_{value}} \times 1.12.$$

Immunostaining. Immunostaining of the platelet endothelial cell adhesion molecule (CD-31/PECAM-1) and zonula occludens 1 (ZO-1) was performed on day 4 after HBMEC seeding to confirm barrier integrity, as detailed previously. The primary antibodies used are listed in Table 1C, while the secondary antibody was Ac Donkey anti-Rb AlexaFluor 546 (Thermo Fisher Scientific). For the semiquantitative analysis of the CD-31 marker (in the presence or absence of fibronectin) in HBMECs, the positive area for this marker was selected in relation to the total area of the region of interest (ROI) and expressed as a percentage of the total area. Image processing and semiquantification of data were performed with the ImageJ software.

Permeability assays and deproteinization of samples

To assess the permeability of HT and Tyr, 1 μM and 10 μM solutions were prepared in the endothelial cell medium. Four days after the triculture establishment, these solutions were added to the apical compartment of the inserts. Basolateral and apical media were collected after 3, 6 and 24 h. Once collected, 100 μL of each sample was taken in a new tube, and 100 μL of cold methanol was added. Samples were vortexed for 2 min and centrifuged at 10 480 G for 5 min.[47] Supernatants were collected and frozen until the day of the analysis.

UPLC-ESI-QqQ-MS/MS analysis

Samples were analyzed using an Acquity I-Class UPLC separation system coupled to a Xevo TQ-XS triple quadrupole mass spectrometer (Waters, Milford, MA, USA) equipped with an electrospray ionization (ESI) source. The column used for the chromatographic separation was reversed-phase Acquity Premier HSS T3 (2.1 mm × 100 mm, 1.8 particle size, Waters). For UPLC, water (eluent A) and acetonitrile (eluent B), both acidified with 0.01% formic acid, were used as mobile phases. The gradient started with 7% B, maintaining isocratic conditions for 3 min, followed by an increase to 15% B at min 7.5, then to 30% B over 0.5 min, continued to 40% B for another 0.5 min, and finally to 95% B over 1.7 min. Then, the system returned to the initial conditions (7% B). Isocratic conditions were maintained for 1.8 min to re-equilibrate the column, resulting in a total run time of 12 min. The flow rate was set to 0.4 mL min^{-1}, the injection volume was 2 μL, and the column temperature was maintained at 40 °C. The MS operated in the negative ionization mode with a desolvation temperature of 600 °C. The source temperature was set to 150 °C, and the source voltage was 2.3 kV. The compounds were monitored in the multiple reaction monitoring (MRM) mode, with up to three molecular transitions. The system was controlled by MassLynx 4.2 software, and the data were processed using TargetLynx XS 4.1.1.0 software (Waters). HT, Tyr and their metabolites were identified by comparison of the retention time and MS/MS fragmentation patterns (m/z) with those of pure commercial analytical standards. Quantification was performed using the calibration curves of the following standards: HT, Tyr, hydroxytyrosol-3′-sulfate, hydroxytyrosol-4′-sulfate, hydroxytyrosol acetate, hydroxytyrosol-3′-glucuronide, hydroxytyrosol-4′-glucuronide, tyrosol-sulfate.

Apparent permeability coefficient (P_{app}) calculations

P_{app} values were calculated following the formula:

$$P_{app}(\mathrm{cm\ s^{-1}}) = \frac{V_r \times (\mathrm{d}Q/\mathrm{d}t)}{C_0 \times A},$$

where V_r is the volume in the receiving chamber (1 mL); $\mathrm{d}Q/\mathrm{d}t$ is the amount of the compound per unit of time; C_0 is the initial concentration on the apical side (1 or 10 μM); and A is the exposed area (1.12 cm^2, the area of the membrane of the transwell system).[48]

Statistical analysis

Statistical analyses were carried out using GraphPad Prism software version 8.0.2 (GraphPad Software, Inc., San Diego, CA, USA). T-Student and one-way ANOVA tests were used to analyze significant differences. The degree of significance of the analysis was as follows: $^{*}p < 0.05$, $^{**}p < 0.01$, $^{***}p < 0.001$ and $^{****}p < 0.0001$. Data are presented as mean ± standard deviation (SD) of triplicates.

Results

Blood–brain barrier model in triculture with primary human cells

One of the principal objectives of this study was to implement an *in vitro* ho-BBB model that could mimic the *in vivo* counterpart. Three primary cell types comprising the neurovascular unit were employed: astrocytes, pericytes, and BMECs of human origin. The different cells were characterized through immunofluorescence against their specific markers: GFAP, PDGFR-β, and CD-31, respectively (Fig. 1).

To develop the model, 12 mm and 3.0 μm pore-size transwell inserts were used. This selection was based on the optimized conditions reported by Stone *et al.* (2019),[44] which demonstrated that significantly higher TEER values were achieved when the pore size was 3.0 μm *vs.* 0.4 μm. This can be explained by an increased contact between the cells in the apical and basolateral sides of the insert, resulting in greater barrier strength.[44]

Preliminary experiments were performed to establish a suitable number of HBMECs. In this sense, 7.5×10^4, 1×10^5, and 1.5×10^5 cells were seeded on the apical side of the transwell inserts (with astrocytes and pericytes on the basolateral side), and TEER values were measured during the following 4 days. 1×10^5 was selected since this density yielded higher TEER values than 7.5×10^4, as at the same time, no significant differences were observed with 1.5×10^5 cells (Fig. 2A). Regarding astrocytes and pericytes, cell seeding densities were those established by Stone *et al.* (2019):[44] 3.13×10^5 for astrocytes and 6.25×10^4 for pericytes, in a ratio of 5 : 1. By comparing our triple-culture ho-BBB model with a monolayer of HBMECs, significantly higher TEER values were obtained (Fig. 2B), which reinforces the advantage of using our ho-BBB model over classic monolayers.

In addition, we evaluated the effect of the presence of fibronectin as an extracellular matrix for endothelial cells. Compared to previous reports by Stone *et al.* (2019),[44] we achieved higher TEER values when using a fibronectin coating on the apical side of the insert. Thus, a greater integrity and a smaller number of gaps were observed with a fibronectin coating measured by immunofluorescence against CD-31, the specific surface marker of HBMECs (Fig. 2C and D). In the presence of fibronectin, the percentage of the positive area increased to approximately 14%, whereas cells cultured without the matrix showed only about 1.9% (Fig. 2E).

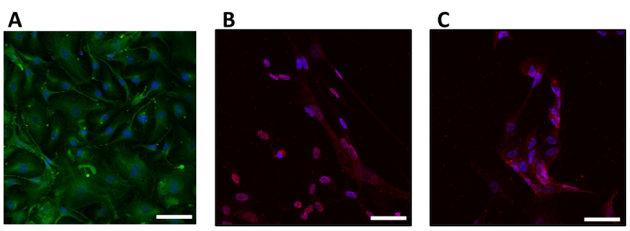

Fig. 1 Immunofluorescence characterization of astrocytes, pericytes, and human brain microvascular endothelial cells (HBMECs) present in the human-origin BBB model. (A) HBMECs stained for evaluating the presence of CD-31. (B) Pericytes stained for evaluating the presence of PDGFRβ. (C) Astrocytes stained for evaluating the presence of GFAP. Nuclei were counterstained with DAPI. Scale bar: 50 μm.

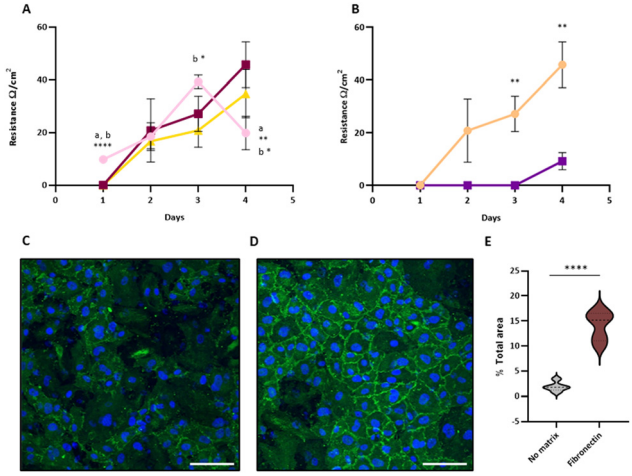

Fig. 2 Tested parameters of the ho-BBB model. (A) TEER values measured in cultures with three different seeding densities (cells per well) of HBMECs (pink circles: 7.5×10^4; red squares: 1×10^5 and yellow triangles: 1.5×10^5). Data are expressed as mean ± SD $n = 3$. Different superscript letters mean significant differences (*$p < 0.05$, **$p < 0.01$, ***$p < 0.001$, and ****$p < 0.0001$) between the samples as follows: [a]7.5×10^4 *vs.* 1×10^5, [b]7.5×10^4 *vs.* 1.5×10^5, and [c]1×10^5 *vs.* 1.5×10^5 (B) TEER values measured in triculture *versus* the monoculture of HBMECs (orange: HBMECs in triculture and purple: HBMECs in monoculture). Data are expressed as mean ± SD $n = 3$. (C) Immunofluorescence staining of CD-31 in HBMECs cultured in the absence of fibronectin and (D) in the presence of fibronectin 96 h after their seeding. Nuclei were counterstained with DAPI. Scale bar: 50 μm. (E) Semiquantitative analysis of CD-31 expression as a percentage of the total area (****$p < 0.0001$).

Based on these results, the ho-BBB model was established as follows: on day 1, the basolateral side of the inserts was coated with a poly-L-lysine solution (2 μg mL^{-1}), and then, 3.13×10^5 astrocytes were seeded on the same side of the insert. On day 2, 6.25×10^4 pericytes were also seeded on the basolateral side of the insert. Fibronectin was added as an extracellular matrix on day 3 as a preliminary step for HBMEC seeding on day 4.

Based on TEER measurements, day 8 (96 h after HBMEC seeding) was established as the appropriate time to perform permeability studies (Fig. 3A). In fact, five days after establishing the triculture, TEER values decreased significantly and continued to decline until day 12 (Fig. S1). Furthermore, the formation of ZO-1 (Fig. 3B) and the expression of the specific surface marker CD-31 on day 8 confirmed the results obtained by TEER measurements (Fig. S2). ZO-1 is a protein indicative of the integrity and functionality of tight junctions between cells. An increase in ZO-1 suggests a stronger barrier and lower permeability through it.

Permeability of Tyr and HT across the BBB

Tyr and HT (Fig. 4A and B) were selected to study the permeability across the BBB. Both compounds were added individually to the upper compartment in two different concen-

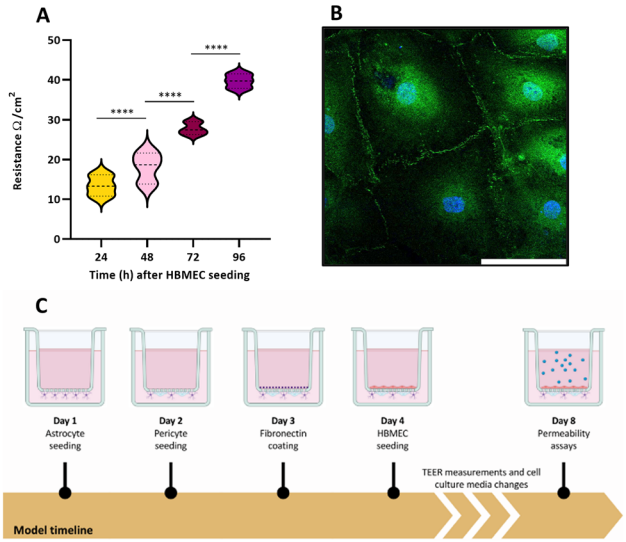

Fig. 3 Protocol for the *in vitro* ho-BBB functionality tests: (A) TEER measurements up to 96 h after HBMEC seeding. Results are expressed as mean ± SD of four independent experiments. (B) Immunofluorescence staining of ZO-1 in the HBMEC monolayer. (C) Schematic of the protocol. Scale bar: 100 μm. Statistical analysis was performed using one-way ANOVA (****$p < 0.0001$).

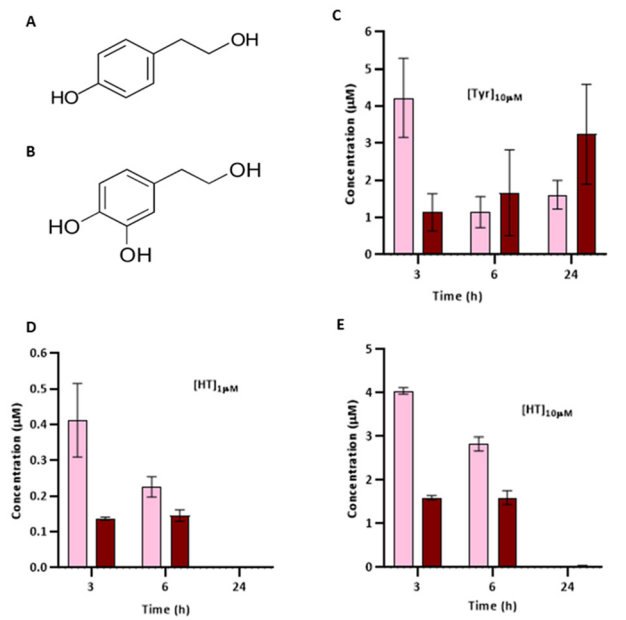

Fig. 4 Chemical structures and permeabilities of Tyr and HT across the ho-BBB. (A) Chemical structure of Tyr. (B) Chemical structure of HT. (C–E) Concentrations (μM) of Tyr and HT measured at different time points in the apical (pink) and basolateral (red) compartments of transwell inserts after apical administration: (C) Tyr after the addition of 10 μM, (D) HT after the addition of 1 μM and (E) HT after the addition of 10 μM. Data are expressed as mean ± SD. $n = 3$.

trations: 1 and 10 μM. These are within the concentration range estimated in human plasma after the consumption of olive oil.[17,49,50] Cell culture media were collected from both sides of the transwell system (apical: blood compartment; basolateral: brain compartment) at different times: 3, 6, and 24 h. 3 h corresponds to the half-life time of these compounds,[29,49] while 6 and 24 h values serve to compare with the existing literature,[30,33] to determine the evolution of the compound over time, and could be useful for studying their further metabolites. After deproteinization of the culture media, the identification and quantification of compounds and metabolites were conducted by UPLC-ESI-QqQ-MS/MS by comparison with pure commercial analytical standards (Table 2, mass spectrum in Fig. S3).

Regarding Tyr, when this bioactive was added at 1 μM, it was not detected on either the basolateral or apical side. However, at 10 μM, Tyr was identified and quantified in both compartments. After 3 h, the Tyr concentration was 4.22 ± 1.07 μM, which decreased significantly (1.15 ± 0.42 μM) after 6 h in the apical side. As expected, the concentration of Tyr in the basolateral side increased over time, reaching the maximum concentration value of 3.24 ± 1.34 μM after 24 h (Fig. 4C). Unlike Tyr, HT could be identified and quantified at both concentrations tested, 1 μM and 10 μM, both following a similar trend. In fact, on the apical side, concentrations gradually decreased until reaching values close to 0 after 24 h (from 0.41 ± 0.10 to 0.00 ± 0.00 (1 μM); from 4.05 ± 0.07 to 0.01 ± 0.00 (10 μM)). However, on the basolateral side, concentrations remained stable for up to 6 h (0.15 ± 0.02 (1 μM) and 1.60 ± 0.16 (10 μM)) and then decreased to values close to 0 after 24 hours (Fig. 4D and E).

Table 3 shows the transport % and P_{app} values for Tyr and HT across the ho-BBB. The transport % indicates the percentage of the compound on the basolateral side relative to the total (the sum of apical and basolateral sides). Tyr at 10 μM exhibited transport % that increased over time, which may indicate that the compound accumulates on the basolateral side. For HT at both concentrations, the transport % also increased over time, with similar values (Table 3). However, after 24 h, practically all HT was found on the basolateral side, which explains the high transport %, even though the concentration values are close to 0, as was described above (Fig. 4D and E).

The P_{app} allows us to classify the permeability of a compound as low ($<2 \times 10^{-6}$), medium ($2–10 \times 10^{-6}$), high ($10–20 \times 10^{-6}$), or very high ($>20 \times 10^{-6}$).[48] Based on these calculations, we observed that the permeability of Tyr was medium at 3, 6 and 24 h (Table 3). In contrast, the permeability of HT was classified as high after 3 h (coinciding with its half-life values)[49] and medium after 6 h. For both compounds, P_{app} values decreased significantly after 24 h.

Capability of BBB to form new brain metabolites from HT

One factor that could be relevant to the permeability of phenolic metabolites across the BBB is the potential metabolic activity of cells. To this end, the main phase II metabolites found in plasma after EVOO consumption (acetyl, sulfate, and glucuronide forms of Tyr and HT, Table 2) were targeted.[51,52] From all those metabolites (Table 2), our results demonstrated

Table 2 Identification and quantification parameters for different compounds analyzed by UPLC-ESI-QqQ-MS/MS

Retention time (min)	Compound[a]	Parent ion [M–H]– (*m*/*z*)	MS/MS fragments (*m*/*z*)		
1.72	Hydroxytyrosol-4′-glucuronide	329	153	123	113
1.97	Hydroxytyrosol-3′-glucuronide	329	153	123	113
2.27	Hydroxytyrosol-4′-sulfate	233	153	123	
2.28	Hydroxytyrosol	153	123	95	
2.49	Hydroxytyrosol-3′-sulfate	233	153	123	
2.61	Tyrosol-sulfate	217	137	119	106
3.21	Tyrosol	137	119	106	
6.15	Hydroxytyrosol-acetate	195	135	123	

[a] Compounds identified using pure commercial standards.

Table 3 Transport percentages (%) and apparent permeability coefficients (P_{app})[a] of HT and Tyr across the ho-BBB

	After 3 h		After 6 h		After 24 h	
	Transport %	P_{app}[a]	Transport %	P_{app}[a]	Transport %	P_{app}[a]
Tyr (1 μM)	—	—	—	—	—	—
Tyr (10 μM)	21.94 ± 11.64	9.46 ± 4.15	56.66 ± 9.37	6.90 ± 4.78	65.28 ± 14.79	3.35 ± 1.36
HT (1 μM)	22.67 ± 4.47	11.10 ± 0.33	30.82 ± 0.42	6.00 ± 0.66	100.00 ± 0	0.00 ± 0.00
HT (10 μM)	19.89 ± 6.28	11.30 ± 0.41	31.43 ± 6.26	6.61 ± 0.66	86.51 ± 3.95	0.04 ± 0.00

[a] P_{app} is expressed as the mean ± SD ($\times 10^{-6}$) cm s^{-1}.

that HT was metabolized by the ho-BBB to form hydroxytyrosol-3′-sulfate (HT-3S) and hydroxytyrosol-4′-sulfate (HT-4S) when HT was added to the apical side at 10 μM (Fig. 5A and B). The concentrations of both metabolites were around 600 times lower than those of HT, ranging from 0.002 to 0.007 μM (Fig. 5C and D) at all-time points. The maximum concentrations of HT-3S and HT-4S (0.007 ± 0.0004 μM and 0.022 ± 0.004 μM, respectively) were achieved after 6 h of incubation with HT (10 μM) on the apical side.

Therefore, the decrease in HT in the apical compartment after 6 h of incubation can be partly explained by the formation of these newly formed sulfate metabolites. The concentrations found on the basolateral side remained constant until 6 h, after which they declined.

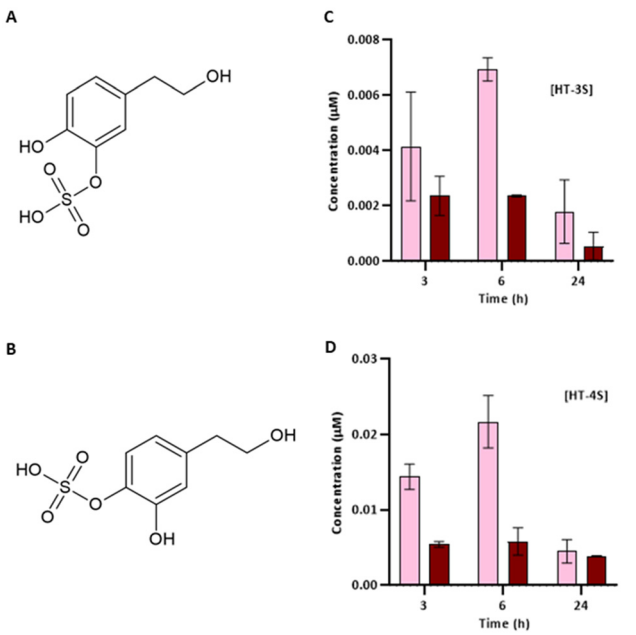

Fig. 5 Concentration of new metabolites formed from HT by the ho-BBB. (A) Chemical structure of HT-3-sulfate. (B) Chemical structure of HT-4-sulfate. (C) Concentration (μM) of HT-3-sulfate measured at different time points in the apical (pink) and basolateral (red) compartments of transwell inserts after the addition of 10 μM HT. (D) Concentration (μM) of HT-4-sulfate measured under the same conditions. Data are expressed as mean ± SD. n = 3.

Discussion

The BBB is composed of BMECs closely associated with supporting cells, including astrocytes and pericytes. While endothelial cells constitute the structural basis of the barrier, interactions with astrocytes and pericytes are essential for the acquisition and maintenance of BBB-specific properties.[23] These supporting cells play critical roles in regulating endothelial function and preserving the integrity of the barrier.

Most of the studies conducted to evaluate the permeability of compounds/drugs have been carried out using endothelial cell monocultures;[29,30,33] however, these systems do not accurately mimic the *in vivo* BBB characteristics. For this reason, the coculture of endothelial cells with astrocytes and pericytes has been increasingly recognized as an effective approach for developing BBB models that better reproduce the physiological characteristics and specialized functions of the native barrier.[43–45] Nevertheless, the utility of this model for asses-

sing the permeability of compounds has not been sufficiently explored.

Another important aspect is the origin of cells. Several BBB models have been developed based on animal cells of porcine or rat origin, which include variations in the expression of transport proteins, functional properties, and species-specific metabolic pathways.[53,54] Such disparities can significantly influence the uptake, efflux, and overall permeability of compounds across the BBB. In the present study, an *in vitro* ho-BBB model was implemented by co-culturing three primary human cell lines (HBMECs, astrocytes and pericytes). The presented model was based on a previous model described by Stone *et al.* (2019),[44] which likewise employed human primary cells, albeit for an application distinct from permeability assessments, as these authors studied the barrier integrity in ischemia, induced by the deprivation of oxygen and glucose. One of the key improvements of our method has been the selection of an optimal seeding density of HBMECs, and the incorporation of an extracellular matrix prior to their culturing.

In our case, the ho-BBB model consisted of 3.13×10^5 astrocytes, 6.25×10^4 pericytes and 1×10^5 HBMECs, which accounts for a ratio of 5 : 1 : 1.5 between these three cells. This is in agreement with previous studies, which indicate that the *in vivo* number of astrocytes exceeds that of HBMECs[55,56] and that the estimated ratio of pericytes to HBMECs is between 1 : 1 and 1 : 3 in mice.[57,58]

Our study demonstrated that a concentration of 1×10^5 cells, in conjunction with the coating of the apical side of the transwell insert with fibronectin, resulted in elevated TEER values and an enhanced integrity of the barrier (Fig. 2). These results are quantitative values that serve as the gold standard for a minimally invasive assessment of BBB integrity.[59] Furthermore, the immunocytochemical analysis of ZO-1 revealed the clear expression of this junctional protein, showing well-defined localization at the cell membrane. This was the first tight junction to be discovered, which is located in the cytosol and has a peripheral membrane location. It has multiple domains that are specialised for protein interactions.[60] The ho-BBB model was considered ready for permeability assays after 96 h of the establishment of the triculture, corresponding to the time point at which TEER measurements reached their peak values (Fig. 3).

Another study developed and compared several configurations for an *in vitro* BBB model with BMECs, astrocytes, and pericytes, but in this case, the cells were immortalised.[43] They fixed the pore size of the inserts (0.4 μm) and assayed different barrier setups, which did not include the co-culturing of astrocytes and pericytes on the same surface. Most of the systems studied by these authors attained TEER values comparable to those obtained in the present study (approximately 78.8 ± 4.2 Ω cm^2),[43] even though our ho-BBB model requires one day less to perform the permeability tests. Noteworthy, they assayed the permeability of drugs (propranolol, pyrilamine, memantine, and diphenhydramine) already known for their ability to pass through the BBB and did not consider food bioactive compounds, and regarding time, they only considered an hour and a half of testing, which is considerably less time than in our study and did not provide time-dependent insights.[43]

It is widely acknowledged that Tyr and mainly HT are food bioactives that have been demonstrated to possess a range of bioactive properties, including anti-oxidant, anti-inflammatory, anti-atherogenic, anti-thrombotic, cardioprotective and chemopreventive effects.[3,61] Furthermore, HT is increasingly recognized for its neuroprotective and anti-neuroinflammatory properties, as proven by quite a number of *in vitro* and *in vivo* assays.[60–65] Mounting evidence supports that these compounds may cross the body's most selective barrier, the BBB. The initial evidence that this compound could reach the brain was documented in 2001 by D'Angelo and colleagues *via* the intravenous injection of ^{14}C -labeled HT (1.5 mg kg^{-1}) in rats.[26] This finding was subsequently confirmed by other authors who found HT in the brain after administering higher doses (100 mg kg^{-1} i.v.).[66] Additionally, some *in vitro* studies have demonstrated the capacity of this phenyl alcohol and its sulfate and glucuronide metabolites to pass through the BBB using BMEC monolayers.[29,30]

A critical element to consider when investigating the brain's penetration of a dietary compound is the concentration found in circulation following its consumption. Plasma concentrations of free HT ranged from 0.03 to 15 μM after consuming between 25 and 40 mL of virgin olive oil.[17,49,50] In addition, our research group estimated a dietary intake of HT of 17.25 mg day^{-1} provided by EVOO (two spoons), wine (two glasses) and olives (7 units), all characteristic foods of the Mediterranean diet. The calculated reported bioavailability for HT is 44%.[64] Taking the plasma volume into account, the estimated circulating HT from dietary sources can be as high as 10.69 μM, which is within the range of our study. This approach was adopted to ensure the physiological relevance of the findings obtained. Consequently, the concentrations of 1 and 10 μM were added on the apical side of the developed ho-BBB model for both Tyr and HT permeability assays. Moreover, three different time points were selected: 3 h (which corresponds to the half-life in plasma for these compounds),[49] 6 h, and 24 h, with the aim of evaluating the effect of time on the permeability of these compounds and to facilitate comparison with the existing literature.[33] The results indicate that adding Tyr (detectable at 10 μM but not at 1 μM) caused a marked decrease on the apical side from 3 to 6 h, with a corresponding increase on the basolateral side (Fig. 4C). HT showed a similar pattern at both 1 and 10 μM, with basolateral concentrations declining to nearly 0 by 24 h. Notably, in the brain compartment, HT levels remained almost unchanged between 3 and 6 h (Fig. 4D and E). It should be noted that in all cases, the sum of the concentrations in the apical and basal compartments did not match the concentration initially added, probably explained by the compounds' instability in cell culture media.[67] Indeed, several articles have demonstrated that phenolic compounds exhibit greater stability within human plasma than culture media, probably caused by polyphenol-protein interactions.[68–70]

Transport % and P_{app} values were calculated based on quantified Tyr and HT concentrations on the apical and basolateral sides. In general, transport % increased over time for Tyr and HT. In the case of HT, similar percentages were observed for both tested concentrations, so a dose-dependent effect was not noted. The BBB transport of Tyr and HT has been recently evaluated in an HBMEC monolayer after the addition of 20 and 2000 μM Tyr and 1 and 100 μM HT, concentrations significantly higher than those evaluated in this study, and after 4 h of incubation. Tyr, at this time, presented a transport % around 30%.[30] Similar values were obtained in this study after 3 h of incubation (22%), but using half the concentration. However, in the case of HT at 1 μM, the results of this paper indicated a transport % value of 70% at 4 h, which is significantly higher than the value calculated in this study (around 25% at 3 h). This phenomenon can be attributed to the structural disparities inherent to the BBB between a three-cell culture and a monoculture. The presence of astrocytes and pericytes in our ho-BBB model demonstrated a significant influence on the integrity of the barrier compared to a monolayer formed solely by HBMECs (Fig. 2B).

A recently published study evaluated the BBB transport (using an HBMEC monolayer) of various phenolic metabolites derived from Tyr and HT, specifically tyrosol-4′-sulfate, HT-3S, and HT-4S, each applied on the apical side of the insert at a concentration of 2.5 μM for 2 h.[29] The findings indicated that the transport % of these sulfate metabolites across the BBB did not exceed 10% in any case, a value comparable to that observed for the corresponding parent compounds examined in the present study.[29] An additional metric used to assess permeability is the transport rate, which is defined as the ratio between the concentration detected at the end of the experiment and the initial concentration applied at 0 h. This parameter has been employed by other investigators to characterize the BBB transport of various flavonoids using co-cultures of rat BMECs and astrocytes. Under these conditions, genistein, isoliquiritigenin, and apigenin exhibited the highest transport rates, ranging from 14% to 29%.[71] In a similar manner, Faria *et al.* determined the transport rates of (+)-catechin and (−)-epicatechin across a monolayer of hCMEC/D3 cells (an immortalized human brain endothelial cell line), reporting transport values of approximately 20% and 25%, respectively.[72]

The apparent permeability coefficient, denoted by P_{app}, is a value that, in contrast to the transport %, considers multiple variables including the initial concentration added, the concentration in the brain compartment, the insert area, and the test time. Consequently, the P_{app} can be considered a more physiologically relevant value, classifying the permeability of a compound/drug as low, medium, high, or very high.[48] For the calculation of the permeability of food bioactives or their metabolites through the BBB, P_{app} is less frequently used than transport %. Our results showed that HT displays the highest values. HT's structure with an *ortho*-diphenolic substitution, compared to a single hydroxyl in Tyr, may explain the higher ability of HT to cross the barrier. Indeed, the most efficient hydrogen-donor systems, such as those with the dihydroxy functionality, allow molecules to cross the barrier more freely.[73]

The present findings provide new evidence of the ability of HT and Tyr to cross the BBB. However, it is important to note that the permeability mechanisms and the specific transporters still need to be fully elucidated. Future studies using transporter inhibitors or transcriptomic profiling of BBB cells may help further elucidate the molecular mechanisms involved in the transport and metabolism of these phenolic compounds. Limited evidence exists on the permeability and transport mechanisms of phenolic compounds.[74–77] Concretely, for HT, previous research employing intestinal cells (Caco-2) indicated that the transport of HT can occur *via* passive diffusion in a bidirectional manner.[74] Another study comprising homovanillic acid (4′-hydroxy-3′-methoxyphenylacetic acid), a chemically similar compound to the ones used in this study (with a carboxylic acid group in the C1 position of the phenolic ring and a methyl group in the C3 position of the phenolic ring), and gallic acid (3,4,5-trihydroxybenzoic acid, with an additional hydroxyl group in the C5 position of the phenolic ring) showed that these compounds can cross the BBB through active transport, triggering the inhibition of solute carrier transporters (SLC), in particular, organic anion transporters (OAT1/SLC22A6 and OAT3/SLC22A8).[76,77]

This ho-BBB model has been utilised to illustrate the BBB's capacity to metabolise HT, resulting in the transformation of HT into sulfate conjugates, namely, HT-3S and HT-4S. The present findings are consistent with the observations reported in rat brains, in which the majority of conjugated metabolites were found to be sulfate derivatives, subsequent to the systemic administration of their respective nonconjugated compounds.[29,41,75]

Existing evidence suggests that metabolizing enzymes including UDP-glucuronosyltransferases, sulfotransferases, glutathione S-transferases, *N*-acetyltransferases, and methyltransferases are present in human brain microvessels, where they exert an effect on limiting the number of toxic substances that enter the brain.[78,79] In fact, SULT1A1 has been detected in human microvessels at the transcriptomic level, which suggests that this enzyme could exert its function in the brain endothelium.[78] Some previous studies have highlighted the potential capacity of BMECs and HBMECs to metabolize phenolic compounds and even their metabolites.[32,33] In fact, Faria and colleagues showed that immortalized BMECs can glucuronidate both (+)-catechin and (−)-epicatechin, which are subsequently detected in the basolateral medium, further supporting the ability of both compounds to cross the barrier.[72] Moreover, it has been proposed that HBMECs metabolize catechol-1-sulfate into novel glutathione and glucuronic acid derivatives. This conversion is attributed to the potential glutathione S-transferase, UDP-glucuronosyl transferase, gamma-glutamyl transpeptidase, and catechol-*O*-methyltransferase activity.[33] Our findings are in accordance with the previous literature, in which the sulfate derivatives of HT have been identified in rat brains after an oral administration of refined

olive oil enriched with HT at different doses.[28,80] Furthermore, it should be noted that HT is an endogenous metabolite of dopamine.[81] This neurotransmitter can undergo sulfation mediated by SULTs in the central nervous system and periphery;[82,83] thus, we can hypothesize that HT could also undergo these conjugation reactions by endothelial cells. Further studies are required to confirm this hypothesis. These studies should evaluate the presence of sulphate enzymes and the metabolic capacity of the cells comprising the neurovascular unit.

Conclusions

A human triculture BBB model comprising primary HBMECs, astrocytes, and pericytes was successfully applied for the first time to evaluate the permeability of dietary phenolics. Preliminary experiments identified 1×10^5 HBMECs as the most suitable seeding density, yielding TEER values comparable to or higher than those of previously established models. The incorporation of fibronectin as an apical extracellular matrix resulted in further strengthening of barrier integrity, thus confirming the added physiological relevance of this system in comparison with conventional endothelial monocultures.

Through the use of this so-called ho-BBB model, we observed distinct permeability profiles for Tyr and HT. Tyr displayed medium permeability through the different time points, whereas HT exhibited an initial high permeability, which declined progressively, suggesting time-dependent metabolic processes. We also demonstrated that the ho-BBB displays metabolic capacity, converting HT into HT-3S and HT-4S and confirming that the BBB can act as an active metabolic interface generating brain-accessible metabolites.

Taken together, the human triple coculture model provides a physiologically relevant platform for studying the permeability and metabolism of dietary bioactives. Further research is required to elucidate the precise mechanisms underlying the BBB transport of Tyr and HT and to determine the biological relevance of the newly formed metabolites. These findings underscore the pivotal role of the BBB-mediated metabolism of dietary phenolics and their potential to exert direct effects on neuronal cells, which may bear significant implications for brain function and the prevention of neurological disorders.

Author contributions

Conceptualization: R. H. O., A. M. T.; formal analysis: S. G. D., M. B., R. H. O.; funding acquisition: R. H. O.; investigation: S. G. D., B. E. L., C. d. R; methodology: S. G. D., R. H. O., A. M. T., P. M.; project administration: R. H. O., A. M. T.; resources: P. M.; supervision: R. H. O., A. M. T., P. M., C. d. R; visualization: S. G. D.; writing – original draft preparation: S. G. D., R. H. O., A. M. T.; writing – review and editing: S. G. D., M. B., R. H. O., A. M. T., B. E. L., C. d. R., J. M., P. M. All authors have read and agreed to the published version of the manuscript.

Conflicts of interest

There are no conflicts to declare.

Data availability

The data that support the findings of this study are available from the corresponding author upon reasonable request.

Supplementary information (SI) is available. Fig. S1. TEER values of the triculture model over a period of 12 days. Fig. S2. HBMECs integral layer 96 h after the establishment of the triculture confirmed by immunofluorescence staining of CD-31 surface marker expression. Fig. S3. MS/MS fragmentation pattern (*m*/*z*) of (A) HT, (B) Tyr, (C) HT-4S and (D) HT-3S. See DOI: https://doi.org/10.1039/d6fo00323k. *m*/*z*) of (A) HT, (B) Tyr, (C) HT-4S and (D) HT-3S.

Acknowledgements

We acknowledge the Biology and Microscopy Services (CITIUS) of the Universidad de Sevilla for the equipment. This research was funded by the Grant PID2022-140326OA-I00 funded by MICIU/AEI/10.13039/501100011033 and FEDER, UE. In addition, we thank the European Research Council (ERC) project under the European Union's Horizon 2020 Research and Innovation Programme (PREDICT-CARE project, grant agreement no 950050). Moreover, we thank the applied research and innovation project (SOL2024-31748, POLIFENEV project), co-financed by the EU–Ministerio de Hacienda y Función Pública-European Funds–Junta de Andalucía-Consejería de Universidad, Investigación e Innovación. S. G. D. and R. H. O. gratefully acknowledge Dr Prof. A. J. Herrera Carmona (Department of Biochemistry and Molecular Biology, University of Seville) for his expert guidance and valuable contribution to the statistical analysis of the data.

References

1 C. Féart, C. Samieri, B. Allès and P. Barberger-Gateau, Potential benefits of adherence to the Mediterranean diet on cognitive health, *Proc. Nutr. Soc.*, 2013, **72**(1), 140–152.
2 C. A. Anastasiou, M. Yannakoulia, M. H. Kosmidis, E. Dardiotis, G. M. Hadjigeorgiou, P. Sakka, *et al.*, Mediterranean diet and cognitive health: Initial results from the Hellenic Longitudinal Investigation of Ageing and Diet, *PLoS One*, 2017, **12**(8), e0182048.
3 M. Bertelli, A. K. Kiani, S. Paolacci, E. Manara, D. Kurti, K. Dhuli, *et al.*, Hydroxytyrosol: A natural compound with

promising pharmacological activities, *J. Biotechnol.*, 2020, **309**, 29–33.
4 A. Boronat, G. Serreli, J. Rodríguez-Morató, M. Deiana and R. de la Torre, Olive Oil Phenolic Compounds' Activity against Age-Associated Cognitive Decline, Clinical and Experimental Evidence, *Antioxidants*, 2023, **12**(7), 1472.
5 M. Servili and G. F. Montedoro, Contribution of phenolic compounds to virgin olive oil quality, *Eur. J. Lipid Sci. Technol.*, 2002, **104**, 602–613.
6 E. Tripoli, M. Giammanco, G. Tabacchi, D. D. Majo, S. Giammanco and M. L. Guardia, The phenolic compounds of olive oil: structure, biological activity and beneficial effects on human health, *Nutr. Res. Rev.*, 2005, **18**(1), 98–112.
7 O. Baccouri, M. Guerfel, B. Baccouri, L. Cerretani, A. Bendini, G. Lercker, *et al.*, Chemical composition and oxidative stability of Tunisian monovarietal virgin olive oils with regard to fruit ripening, *Food Chem.*, 2008, **109**(4), 743–754.
8 S. Cicerale, X. A. Conlan, N. W. Barnett, A. J. Sinclair and R. S. J. Keast, Influence of heat on biological activity and concentration of oleocanthal - A natural anti-inflammatory agent in virgin olive oil, *J. Agric. Food Chem.*, 2009, **57**(4), 1326–1330.
9 W. Kamm, F. Dionisi, C. Hischenhuber and K. H. Enge, Authenticity assessment of fats and oils, *Food Rev. Int.*, 2001, **17**(3), 249–290.
10 D. Trombetta, A. Smeriglio, D. Marcoccia, S. V. Giofrè, G. Toscano, F. Mazzotti, A. Giovanazzi and S. Lorenzetti, Analytical evaluation and antioxidant properties of some secondary metabolites in northern Italian mono-and multivarietal extra virgin olive oils (EVOOs) from early and late harvested olives, *Int. J. Mol. Sci.*, 2017, **18**, 797.
11 M. Gallardo-Fernández, M. Gonzalez-Ramirez, A. B. Cerezo, A. M. Troncoso and M. C. Garcia-Parrilla, Hydroxytyrosol in Foods: Analysis, Food Sources, EU Dietary Intake, and Potential Uses, *Foods*, 2022, **11**(15), 2355.
12 M. Morvaridzadeh, M. Alami, N. Zoubdane, H. Sidibé, H. Berrougui, T. Fülöp, *et al.*, High-Tyrosol/Hydroxytyrosol Extra Virgin Olive Oil Enhances Antioxidant Activity in Elderly Post-Myocardial Infarction Patients, *Antioxidants*, 2025, **14**(7), 867.
13 A. K. Kiritsakis, K. A. Kiritsakis and C. K. Tsitsipas, A review of the evolution in the research of antioxidants in olives and olive oil during the last four decades, *J. Food Bioact.*, 2020, **11**, 31–56.
14 M. Brenes and A. D. Castro, Transformation of oleuropein and its hydrolysis products during Spanish-style green olive processing, *J. Sci. Food Agric.*, 1998, **77**(3), 353–358.
15 J. Rodríguez-Morató, A. Boronat, A. Kotronoulas, M. Pujadas, A. Pastor, E. Olesti, *et al.*, Metabolic disposition and biological significance of simple phenols of dietary origin: hydroxytyrosol and tyrosol, *Drug Metab. Rev.*, 2016, **48**, 218–236.
16 EFSA, Scientific Opinion on the substantiation of health claims related to polyphenols in olive and protection of LDL particles from oxidative damage (ID 1333, 1638, 1639, 1696, 2865), maintenance of normal blood HDL cholesterol concentrations (ID 1639), maintenance of normal blood pressure (ID 3781), "anti-inflammatory properties" (ID 1882), "contributes to the upper respiratory tract health" (ID 3468), "can help to maintain a normal function of gastrointestinal tract" (3779), and "contributes to body defences against external agents" (ID 3467) pursuant to Article 13(1) of Regulation (EC) No 1924/2006, *EFSA J.*, 2011, **9**, 2033.
17 A. Pastor, J. Rodríguez-Morató, E. Olesti, M. Pujadas, C. Pérez-Mañá, O. Khymenets, *et al.*, Analysis of free hydroxytyrosol in human plasma following the administration of olive oil, *J. Chromatogr. A*, 2016, **1437**, 183–190.
18 F. Casamenti, C. Grossi, S. Rigacci, D. Pantano, I. Luccarini and M. Stefani, Oleuropein Aglycone: A Possible Drug against Degenerative Conditions. In Vivo Evidence of its Effectiveness against Alzheimer's Disease, *J. Alzheimer's Dis.*, 2015, **45**, 679–688.
19 C. Valls-Pedret, A. Sala-Vila, M. Serra-Mir, D. Corella, R. de la Torre, M. A. Martínez-González, *et al.*, Mediterranean Diet and Age-Related Cognitive Decline A Randomized Clinical Trial, *JAMA Intern. Med.*, 2015, **175**(7), 1094–1103.
20 O. M. Shannon, J. M. Ranson, S. Gregory, H. Macpherson, C. Milte, M. Lentjes, *et al.*, Mediterranean diet adherence is associated with lower dementia risk, independent of genetic predisposition: findings from the UK Biobank prospective cohort study, *BMC Med.*, 2023, **21**(1), 81.
21 J. Peyrol, C. Riva and M. J. Amiot, Hydroxytyrosol in the prevention of the metabolic syndrome and related disorders, *Nutrients*, 2017, **9**(3), 306.
22 M. Robles-Almazan, M. Pulido-Moran, J. Moreno-Fernandez, C. Ramirez-Tortosa, C. Rodriguez-Garcia, J. L. Quiles, *et al.*, Hydroxytyrosol: Bioavailability, toxicity, and clinical applications, *Food Res. Int.*, 2018, **105**, 654–667.
23 N. J. Abbott, A. A. K. Patabendige, D. E. M. Dolman, S. R. Yusof and D. J. Begley, Structure and function of the blood-brain barrier, *Neurobiol. Dis.*, 2010, **37**, 13–25.
24 Y. He, Y. Yao, S. E. Tsirka and Y. Cao, Cell-culture models of the blood-brain barrier, *Stroke*, 2014, **45**, 2514–2526.
25 M. Le Sayec, D. Carregosa, K. Khalifa, C. de Lucia, D. Aarsland, C. N. Santos and A. Rodriguez-Mateos, Identification and quantification of (poly)phenol and methylxanthine metabolites in human cerebrospinal fluid: evidence of their ability to cross the BBB, *Food Funct.*, 2023, **14**(19), 8893–8902.
26 S. D'Angelo, C. Manna, V. Migliardi, O. Mazzoni, P. Morrica, G. Capasso, *et al.*, Pharmacokinetics and metabolism of hydroxytyrosol, a natural antioxidant from olive oil, *Drug Metab. Dispos.*, 2001, **29**(11), 1492–1498.
27 A. Serra, L. Rubió, X. Borràs, A. Macià, M. P. Romero and M. J. Motilva, Distribution of olive oil phenolic compounds in rat tissues after administration of a phenolic extract from olive cake, *Mol. Nutr. Food Res.*, 2012, **56**(3), 486–496.

28 M. López de las Hazas, J. Godinho-Pereira, A. Macià, A. F. Almeida, M. R. Ventura, M. J. Motilva, *et al.*, Brain uptake of hydroxytyrosol and its main circulating metabolites: Protective potential in neuronal cells, *J. Funct. Foods*, 2018, **46**, 110–117.

29 M. Á. Ávila-Gálvez, B. Garay-Mayol, A. Marín, M. A. Brito, J. A. Giménez-Bastida, J. C. Espín, *et al.*, Metabolic Profiling of a Mediterranean-Inspired (Poly)phenol-Rich Mixture in the Brain: Perfusion Effect and *In Vitro* Blood-Brain Barrier Transport Validation, *J. Agric. Food Chem.*, 2025, **73**(18), 11056–11066.

30 M. Gallardo-Fernandez, A. R. Garcia, R. Hornedo-Ortega, A. M. Troncoso, M. C. Garcia-Parrilla and M. A. Brito, *In vitro* study of the blood-brain barrier transport of bioactives from Mediterranean foods, *Food Funct.*, 2024, **15**(7), 3420–3432.

31 J. Weng, X. Shen, R. Wang, L. Lin, X. Tang, C. Xiao, C. Lai and Y. Gao, Pharmacokinetic changes and mechanisms of salisroside in hypobaric hypoxic environment: A LC-MS and proteomics study, *J. Ethnopharmacol.*, 2026, **360**, 121205.

32 A. Faria, M. Meireles, I. Fernandes, C. Santos-Buelga, S. Gonzalez-Manzano, M. Dueñas, *et al.*, Flavonoid metabolites transport across a human BBB model, *Food Chem.*, 2014, **149**, 190–196.

33 I. Figueira, G. Garcia, R. C. Pimpão, A. P. Terrasso, I. Costa, A. F. Almeida, *et al.*, Polyphenols journey through blood-brain barrier towards neuronal protection, *Sci. Rep.*, 2017, **7**(1), 11456.

34 H. Hundsberger, A. Stierschneider, V. Sarne, D. Ripper, J. Schimon, H. P. Weitzenböck, *et al.*, Concentration-dependent pro-and antitumor activities of quercetin in human melanoma spheroids: Comparative analysis of 2d and 3d cell culture models, *Molecules*, 2021, **26**(3), 717.

35 M. Ercelik, C. Tekin, G. Tezcan, S. Ak Aksoy, A. Bekar, H. Kocaeli, *et al.*, Olea europaea Leaf Phenolics Oleuropein, Hydroxytyrosol, Tyrosol, and Rutin Induce Apoptosis and Additionally Affect Temozolomide against Glioblastoma: In Particular, Oleuropein Inhibits Spheroid Growth by Attenuating Stem-like Cell Phenotype, *Life*, 2023, **13**(2), 470.

36 S. Hernández-García, B. García-Cano, P. Martínez-Rodríguez, P. Henarejos-Escudero and F. Gandía-Herrero, Olive oil tyrosols reduce α-synuclein aggregation *in vitro* and *in vivo* after ingestion in a *Caenorhabditis elegans* Parkinson's model, *Food Funct.*, 2024, **15**(13), 7214–7223.

37 M. Jacomelli, V. Pitozzi, M. Zaid, M. Larrosa, G. Tonini, A. Martini, *et al.*, Dietary extra-virgin olive oil rich in phenolic antioxidants and the aging process: long-term effects in the rat, *J. Nutr. Biochem.*, 2010, **21**(4), 290–296.

38 L. Fan, Y. Peng and X. Li, Brain regional pharmacokinetics of hydroxytyrosol and its molecular mechanism against depression assessed by multi-omics approaches, *Phytomedicine*, 2023, **1**, 112.

39 I. Kundisová, H. Colom, M. E. Juan and J. M. Planas, Pharmacokinetics of Hydroxytyrosol and Its Sulfate and Glucuronide Metabolites after the Oral Administration of Table Olives to Sprague-Dawley Rats, *J. Agric. Food Chem.*, 2024, **72**(4), 2154–2164.

40 J. T. Weber, Methodologies and limitations in the analysis of potential neuroprotective compounds derived from natural products, *New Horiz. Transl. Med.*, 2015, **2**(3), 81–85.

41 D. Angelino, D. Carregosa, C. Domenech-Coca, M. Savi, I. Figueira, N. Brindani, *et al.*, 5-(Hydroxyphenyl)-γ-valerolactone-sulfate, a key microbial metabolite of flavan-3-ols, is able to reach the brain: Evidence from different in silico, *in vitro* and *in vivo* experimental models, *Nutrients*, 2019, **11**(11), 2678.

42 M. Á. Ávila-Gálvez, D. Marques, I. Figueira, K. Cankar, D. Bosch, M. A. Brito, *et al.*, Costunolide and parthenolide: Novel blood-brain barrier permeable sesquiterpene lactones to improve barrier tightness, *Biomed. Pharmacother.*, 2023, **167**, 115413.

43 R. Ito, K. Umehara, S. Suzuki, K. Kitamura, K. I. Nunoya, Y. Yamaura, *et al.*, A Human Immortalized Cell-Based Blood-Brain Barrier Triculture Model: Development and Characterization as a Promising Tool for Drug-Brain Permeability Studies, *Mol. Pharm.*, 2019, **16**(11), 4461–4471.

44 N. L. Stone, T. J. England and S. E. O'Sullivan, A novel transwell blood brain barrier model using primary human cells, *Front. Cell. Neurosci.*, 2019, **13**, 230.

45 C. I. Harding, N. R. O'Hare, M. Vigliotti, A. Caraballo, C. I. Lee, K. Millican, I. M. Herman and E. E. Ebong, Developing a transwell millifluidic device for studying blood-brain barrier endothelium, *Lab Chip*, 2022, **22**(23), 4603–4620.

46 N. Hajji, J. Garcia-Revilla, M. S. Soto, R. Perryman, J. Symington, C. C. Quarles, *et al.*, Arginine deprivation alters microglial polarity and synergizes with radiation to eradicate non-arginine-auxotrophic glioblastoma tumors, *J. Clin. Invest.*, 2022, **132**(6), e142137.

47 R. Sala, P. Mena, M. Savi, F. Brighenti, A. Crozier, M. Miragoli, *et al.*, Urolithins at physiological concentrations affect the levels of pro-inflammatory cytokines and growth factor in cultured cardiac cells in hyperglucidic conditions, *J. Funct. Foods*, 2015, **15**, 97–105.

48 D. A. Volpe, Application of method suitability for drug permeability classification, *AAPS J.*, 2010, **12**, 670–678.

49 E. Miró-Casas, M. I. Covas, M. Farre, M. Fito, J. Ortuño, T. Weinbrenner, *et al.*, Hydroxytyrosol disposition in humans, *Clin. Chem.*, 2003, **49**(6), 945–952.

50 M. I. Covas, K. de la Torre, M. Farré-Albaladejo, J. Kaikkonen, M. Fitó, C. López-Sabater, *et al.*, Postprandial LDL phenolic content and LDL oxidation are modulated by olive oil phenolic compounds in humans, *Free Radicals Biol. Med.*, 2006, **40**(4), 608–616.

51 M. Suárez, R. M. Valls, M. P. Romero, *et al.*, Bioavailability of phenols from a phenol-enriched olive oil, *Br. J. Nutr.*, 2011, **106**(11), 1691–1701.

52 L. Rubió, M. Farràs, R. de la Torre, A. Macià, M. P. Romero, R. M. Valls, R. Solà, M. Farré, M. Fitó and M. J. Motilva, Metabolite profiling of olive oil and thyme phenols after a

sustained intake of two phenol-enriched olive oils by humans: Identification of compliance markers, *Food Res. Int.*, 2014, **65**, 59–68.

53 M. Thomsen, N. Humle, E. Hede, T. Moos, A. Burkhart and L. Thomsen, The blood-brain barrier studied *in vitro* across species, *PLoS One*, 2021, **16**(3), e0236770.

54 M. Radan, T. Djikic, D. Obradovic and K. Nikolic, Application of *in vitro* PAMPA technique and in silico computational methods for blood-brain barrier permeability prediction of novel CNS drug candidates, *Eur. J. Pharm. Sci.*, 2022, **168**, 106056.

55 C. Erö, M. O. Gewaltig, D. Keller and H. Markram, A Cell Atlas for the Mouse Brain, *Front. Neuroinform.*, 2018, **12**, 84.

56 A. Das Gupta, L. Asan, J. John, C. Beretta, T. Kuner and J. Knabbe, Accurate classification of major brain cell types using *in vivo* imaging and neural network processing, *PLoS Biol.*, 2023, **21**(11), e3002357.

57 D. E. Sims, The pericyte – A review, *Tissue Cell*, 1986, **18**(2), 153–174.

58 T. M. Mathiisen, K. P. Lehre, N. C. Danbolt and O. P. Ottersen, The perivascular astroglial sheath provides a complete covering of the brain microvessels: an electron microscopic 3D reconstruction, *Glia*, 2010, **58**(9), 1094–1103.

59 L. O'Halloran, O. Akinsete, A. L. Kogan, M. Wrona and A. F. Mahdi, 3D *in vitro* blood-brain barrier models: recent advances and their role in brain disease research and therapy, *Front. Pharmacol.*, 2025, **16**, 1637602.

60 W. T. Kuo, M. A. Odenwald, J. R. Turner and L. Zuo, Tight junction proteins occludin and ZO-1 as regulators of epithelial proliferation and survival, *Ann. N. Y. Acad. Sci.*, 2022, **1514**(1), 21–33.

61 Y. Zhang, H. Xiao, X. Lv, D. Wang, H. Chen and F. Wei, Comprehensive review of composition distribution and advances in profiling of phenolic compounds in oilseeds, *Front. Nutr.*, 2022, **9**, 1044871.

62 C. Angeloni, M. Malaguti, M. C. Barbalace and S. Hrelia, Bioactivity of olive oil phenols in neuroprotection, *Int. J. Mol. Sci.*, 2017, **18**(11), 2230.

63 R. Hornedo-Ortega, A. B. Cerezo, R. M. de Pablos, S. Krisa, T. Richard, M. C. García-Parrilla, *et al.*, Phenolic compounds characteristic of the mediterranean diet in mitigating microglia-mediated neuroinflammation, *Front. Cell. Neurosci.*, 2018, **12**, 373.

64 M. Gallardo-Fernández, R. Hornedo-Ortega, I. M. Alonso-Bellido, J. A. Rodríguez-Gómez, A. M. Troncoso, M. C. García-Parrilla, *et al.*, Hydroxytyrosol decreases lps- and α-synuclein-induced microglial activation *in vitro*, *Antioxidants*, 2020, **9**(1), 36.

65 C. Chen, Q. Ai and Y. Wei, Potential role of hydroxytyrosol in neuroprotection, *J. Funct. Foods*, 2021, **82**, 104506.

66 Y. T. Wu, L. C. Lin and T. H. Tsai, Measurement of free hydroxytyrosol in microdialysates from blood and brain of anesthetized rats by liquid chromatography with fluorescence detection, *J. Chromatogr. A*, 2009, **1216**(16), 3501–3507.

67 G. Aragonès, F. Danesi, D. Del Rio and P. Mena, The importance of studying cell metabolism when testing the bioactivity of phenolic compounds, *Trends Food Sci. Technol.*, 2017, **69**, 230–242.

68 D. Zou and A. Xie, Influence of Polyphenol-plasma Protein Interaction on the Antioxidant Properties of Polyphenols, *Curr. Drug Metab.*, 2013, **14**(4), 451–455.

69 T. Mao, F. N. U. Akshit, I. Matiwalage, S. Sasidharan, C. M. Álvarez, P. Wescombe, *et al.*, Preferential Binding of Polyphenols in Blackcurrant Extracts with Milk Proteins and the Effects on the Bioaccessibility and Antioxidant Activity of Polyphenols, *Foods*, 2024, **13**(4), 515.

70 Z. Zhang, B. Chen, Q. Lin, X. Li, H. Zhang, D. J. McClements, *et al.*, Cyclodextrin regulates the binding of quercetin to plasma proteins: Potentially enhancing bioavailability and efficacy, *Food Biosci.*, 2025, **63**, 105770.

71 Y. Yang, L. Bai, X. Li, J. Xiong, P. Xu, C. Guo and M. Xue, Transport of active flavonoids, based on cytotoxicity and lipophilicity: an evaluation using the blood-brain barrier cell and Caco-2 cell models, *Toxicol. In Vitro*, 2014, **28**(3), 388–396.

72 A. Faria, D. Pestana, D. Teixeira, P. O. Couraud, I. Romero, B. Weksler, *et al.*, Insights into the putative catechin and epicatechin transport across blood-brain barrier, *Food Funct.*, 2011, **2**(1), 39–44.

73 R. Rezaei-Sadabady, N. Zarghami, A. Barzegar, A. Eidi, A. Akbarzadeh and M. Rezaei-Tavirani, Studies of the Relationship between Structure and Antioxidant Activity in Interesting Systems, Including Tyrosol, Hydroxytyrosol Derivatives Indicated by Quantum Chemical Calculations, *Soft*, 2013, **02**(03), 13–18.

74 C. Manna, P. Galletti, G. Maisto, V. Cucciolla, S. D'Angelo and V. Zappia, Transport mechanism and metabolism of olive oil hydroxytyrosol in Caco-2 cells, *FEBS Lett.*, 2000, **470**, 341–344.

75 R. Carecho, D. Marques, D. Carregosa, D. Masuero, M. Garcia-Aloy, F. Tramer, S. Passamonti, U. Vrhovsek, M. R. Ventura, M. A. Brito, C. Nunes Dos Santos and I. Figueira, Circulating low-molecular-weight (poly)phenol metabolites in the brain: unveiling *in vitro* and *in vivo* blood-brain barrier transport, *Food Funct.*, 2024, **15**(15), 7812–7827.

76 S. Mori, H. Takanaga, S. Ohtsuki, T. Deguchi, Y. S. Kang, K. Hosoya and T. Terasaki, Rat organic anion transporter 3 (rOAT3) is responsible for brain-to-blood efflux of homova nillic acid at the abluminal membrane of brain capillary endothelial cells, *J. Cereb. Blood Flow Metab.*, 2003, **23**(4), 432–440.

77 Z. Li, X. Du, Y. Li, R. Wang, C. Liu, Y. Cao, W. Wu, J. Sun, B. Wang and Y. Huang, Pharmacokinetics of gallic acid and protocatechuic acid in humans after dosing with Relinqing (RLQ) and the potential for RLQ-perpetrated drug-drug interactions on organic anion transporter (OAT) 1/3, *Pharm. Biol.*, 2021, **59**(1), 757–768.

78 R. Shawahna, Y. Uchida, X. Declèves, S. Ohtsuki, S. Yousif, S. Dauchy, *et al.*, Transcriptomic and quantitative proteomic analysis of transporters and drug metabolizing enzymes in freshly isolated human brain microvessels, *Mol. Pharm.*, 2011, **8**(4), 1332–1341.

79 M. Ouzzine, S. Gulberti, N. Ramalanjaona, J. Magdalou and S. Fournel-Gigleux, The UDP-glucuronosyltransferases of the blood-brain barrier: their role in drug metabolism and detoxication, *Front. Cell. Neurosci.*, 2014, **8**, 349.

80 M. C. López de las Hazas, C. Piñol, A. Macià, M. P. Romero, A. Pedret, R. Solà, *et al.*, Differential absorption and metabolism of hydroxytyrosol and its precursors oleuropein and secoiridoids, *J. Funct. Foods*, 2016, **22**, 52–63.

81 T. Hashimoto, M. Ibi, K. Matsuno, S. Nakashima, T. Tanigawa, T. Yoshikawa and C. Yabe-Nishimura, An endogenous metabolite of dopamine, 3,4-dihydroxyphenylethanol, acts as a unique cytoprotective agent against oxidative stress-induced injury, *Free Radicals Biol. Med.*, 2004, **36**(5), 555–564.

82 P. Uutela, R. Reinilä, K. Harju, P. Piepponen, R. A. Ketola and R. Kostiainen, Analysis of intact glucuronides and sulfates of serotonin, dopamine, and their phase I metabolites in rat brain microdialysates by liquid chromatography-tandem mass spectrometry, *Anal. Chem.*, 2009, **81**(20), 8417–8425.

83 T. Suominen, P. Uutela, R. A. Ketola, J. Bergquist, L. Hillered, M. Finel, H. Zhang, A. Laakso and R. Kostiainen, Determination of Serotonin and Dopamine Metabolites in Human Brain Microdialysis and Cerebrospinal Fluid Samples by UPLC-MS/MS: Discovery of Intact Glucuronide and Sulfate Conjugates, *PLoS One*, 2013, **8**(6), e68007.

